IOP Conf. Series: Materials Science and Engineering **231** (2017) 012155 doi:10.1088/1757-899X/231/1/012155

Mechanical properties research of the cassette balance for impulse wind tunnel based on inertia compensation

X Q Zhang [1], **J Z Lv** [1,2], **and Y C Wu**[1]

[1] Scienceand Technologyon Scramjet Laboratory, Hypervelocity Aerodynamics Institute CARDC, Mianyang 621000, China
[2] Tribology Research Institute, Mechanical Engineering School, Southwest Jiaotong University, Chengdu, 610031, China

Abstract. The aerodynamic load signals acquired though the cassette force balance is transient while the model was tested in an impulse combustion wind tunnel. Therefore, it is necessary to explore the dynamic properties of the force balance. Firstly, it is simplified as a springs-damping-beam system, and then, the dynamic equation is deduced. Secondly, the mechanical properties of the force balance are researched through the finite element method. The output histories of the balance under step and sine loading are acquired. Results show that the mean elastic output of the balance approximates to the load exerting on it. Furthermore, the inertia compensation could not only improve the accuracy of mean output significantly, but also could reduce the transient error between output and input sharply.

1. Introduction

The shock [1,2] and impulse tunnel [3~5] are the most important ground test facilities for the development of the hypersonic technology. Since the test duration is extremely short which ranges from tens of microseconds to hundreds of milliseconds, the vibration of the test model excited by the transient flow during start period could not settle down and the signals acquired are transient. Therefore, the dynamic properties of the force measurement system should meet the test requirement of an impulse wind tunnel. However, the formula of the balance is acquired through static calibration, without considering dynamic calibration. Consequently, this will bring errors in force measurement.

In order to improve the accuracy of measuring force in a shock or impulse wind tunnel, many scholars proposed some methods which include the accelerator force balance [6-12,14], the strain wave force balance [4,13~14], the optical force balance [15,16], and the piezoelectric force balance [17]. However, all the above balances are employed in shock tunnel whose test durations are lower than 10 milliseconds and whose test models are less than 20kg. But with the development of the hypersonic technology, the test duration can be over 100 milliseconds, such as the Φ2.4m impulse combustion wind tunnel built in the Chinese Aerodynamic Research and Development Center (CARDC) and the JF12 shock tunnel built in the Institute of Mechanics, Chinese Academy of Sciences. Also, the weight of the test model for the Φ2.4m impulse combustion wind tunnel can be over 1,000kg. And these two features make the stain gauge balance to be the only choice for the force-measurement system. Wang [18,19] has acquired the aerodynamics load in JF12 through this method. This shows that it is feasible to consider mean elastic output of the stain-gauge balance as the aerodynamic load to some degree. In order to further improve the accuracy of force measurement and research the transient properties of the aerodynamic load during the test, the inertia compensation is compulsory. So, this paper does transient research on the single and three components stain-gauge balance based on the inertia compensation method.

2. Summary of the cassette stain gauge force balance

The objects researched in this paper are the single and three components cassette stain gauge force balance. As shown in Figure 1,the left one is a single component balance and the right one is the three. They are consisted of the float frame, the fix frame and the measurement elements. The float frame contact with a test model and the fix frame contact with the pedestal of a wind tunnel by screws. The measurement elements of the balance bear deformations while the transient aerodynamic load exerted on the test model. The stain of the measurement elements is acquired by the stain gauge and output by the Wheatstone bridge. Finally, the aerodynamic load is calculated through the mean stain voltages and the coefficient of the balance.

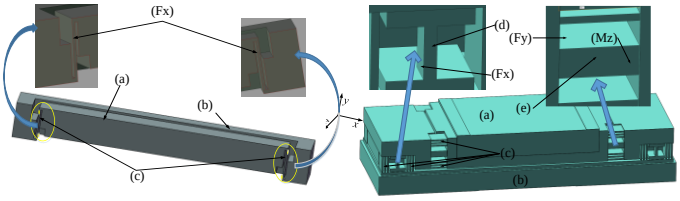

Figure 1 The structure of a single and three components cassette stain gauge balance (a) float frame (b) fix frame (c) F_x measurement elements (d) F_y measurement elements (d) M_z measurement elements

3. Modeling of the force balance

The simplification of the force balance is shown in Figure 2(a), both the support and measurement elements of the balance are thin beams and whose weight are quite little compared with the float and the fix frame and could be ignored. Consequently, they are reduced to the springs with one or three components stiffness. Respectively, the fix frame is rooted and the float frame is hanging during the test time. So, the balance could be further simplified into Figure 2(b), where, $k1_x$, $k1_y$, $k1_{Mz}$ are equal to $k2_x$, $k2_y$, $k2_{Mz}$. The fix frame is reduced to ground and the float frame is reduced to a beam which supported with k1 and k2.

The dynamic equation of the force balance deduced according to Figure 2(b) is following:

$$\boldsymbol{M}\ddot{\boldsymbol{q}} + \boldsymbol{C}\dot{\boldsymbol{q}} + \boldsymbol{K}\boldsymbol{q} = \boldsymbol{F} \tag{1}$$

Where, $\boldsymbol{M}$、$\boldsymbol{C}$、$\boldsymbol{K}$ are the globe mass, damping and stiffness matrix of the force balance, $\boldsymbol{q}$ is the vector of nodal displacements, $\boldsymbol{F}$ is the vector of aerodynamic load. The equation shows that the aerodynamic load exerted on the test model equal to the sum of the elastic, the damping and the inertia load. Thereby, the inertia load is taken into consideration in this paper while damping load is quite small and ignored.

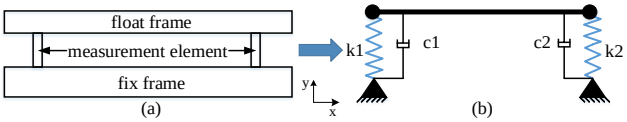

Figure 2 Simplified model of force balance

4. Simulation analysis

4.1 Static virtual calibration

To explore the elastic output of the force balances, it is necessary to calibrate them first. In this paper, the finite element method is applied to acquire the formula and the coefficients of the balance. The positions of the stain gauge are shown in Figure 3. For the single component balance, there are only four stain gauges as shown in Figure 3(a). Meanwhile, for the three components balance there are 24 stain gauges, where 11~18 detect the drag F_x, 21~28 detect the lift F_y, and 61~68 detect the pitching moment M_z. Respectively, all the electric circuit are full Wheatstone bridge. The static calibration formula of balance is:

$$\boldsymbol{F} = \boldsymbol{U} \bullet \boldsymbol{X} \tag{2}$$

For the single component balance, $\boldsymbol{U}=2/4\times10^6\times(-\mu_1+\mu_2-\mu_3+\mu_4)$, while for the three components one,

$$\boldsymbol{F}=\begin{pmatrix}F_x\\F_y\\M_z\end{pmatrix},\ \boldsymbol{U}=\frac{2}{4}\times10^6\times\begin{pmatrix}\mu_{11}+\mu_{12}-\mu_{13}-\mu_{14}+\mu_{15}+\mu_{16}-\mu_{17}-\mu_{18}\\\mu_{21}+\mu_{22}-\mu_{23}-\mu_{24}+\mu_{25}+\mu_{26}-\mu_{27}-\mu_{28}\\\mu_{61}+\mu_{62}-\mu_{63}-\mu_{64}+\mu_{65}+\mu_{66}-\mu_{67}-\mu_{68}\end{pmatrix},\quad \boldsymbol{X}=\begin{pmatrix}x_{11}&x_{12}&x_{13}\\x_{21}&x_{22}&x_{23}\\x_{61}&x_{62}&x_{63}\end{pmatrix}$$

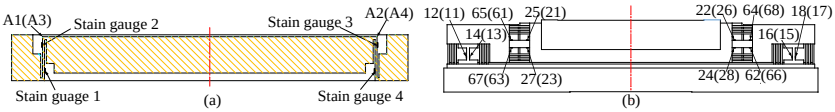

Figure 3 Stain and accelerate detect points of balance (a) single component balance (b) three components balance

4.1.1. Static calibration result of the single component balance. Figure 4(a) shows the finite element model of the single component force balance which embrace 24,000 nodes and 3,500 elements. It is made of Ni18Co8Mo5TiAl whose density is 8,000kg/m^3, Young's Modulus is 187.25GPa and Poisson's Ratio is 0.27. The boundary condition is consists with operating and the drag loading on the upper surface is 1,000N. Figure 4(b) shows the stain result in y direction of the balance, and the stains of points 1~4 are -1.016×10^{-3}, 1.005×10^{-3}, -1.001×10^{-3} and 1.016×10^{-3}. Substitute these data into equation (2) and the coefficient of balance is 0.49472.

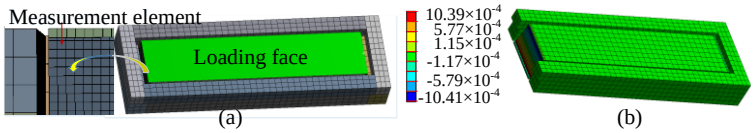

Figure 4 Virtual calibration of single component balance (a) finite element model (b) result of static structural analysis

4.1.2. Static calibrate result of the three components balance. Figure 5(a) shows the finite element model of the three components balance which embrace 111,400 nodes and 17,000 elements. The boundary condition is consistent with its operating, too. And the drag, lift load and the pitching moment loading on the upper surface are 1,000N, 5,000N and 1,000Nm, respectively. Figure 5(b) shows the analysis result. The stain matrix $\boldsymbol{U}$ and the coefficient matrix $\boldsymbol{X}$ we get through equation (2) are as following:

$$\boldsymbol{U}=\begin{pmatrix}477.235&-0.0003&-1.6861\\-0.02065&511.695&-0.015\\13.707&-0.02&486.585\end{pmatrix},\quad \boldsymbol{X}=\begin{pmatrix}2.10&7.56\times10^{-6}&7.26\times10^{-3}\\8.28\times10^{-5}&9.77&6.05\times10^{-5}\\-5.90\times10^{-2}&4.01\times10^{-4}&2.05\end{pmatrix}$$

As shown in coefficient matrix $\boldsymbol{X}$, x_{13} and x_{61} are much larger than other cross interference coefficients except principal coefficients. This illustrates that the cross interference between the drag and the pitching moment is more strong. Meanwhile, the other coefficients x_{12}, x_{21}, x_{23} and x_{32} are relatively small, this demonstrates that the interference between the drag or the pitching moment and the lift is relatively weak. In a word, the coupling between the drag and the pitching moment is more serious than that between the lift and the drag or the pitching moment.

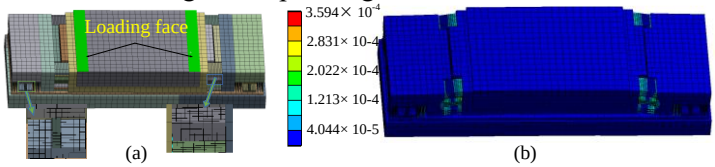

Figure 5 Virtual calibration of three components balance (a) finite element model (b) result of static structural analysis

4.2 The load of transient analysis

Figure 6 shows the total pressure of the test section and the drag voltage output during the 5m standard model test in the impulse wind tunnel. As shown in this figure, the total pressure of the test section climbs after the wind tunnel start up, and last a time of 400 ms. Therefore, the step load must be taken into consideration while researching the mechanical properties of the force balance.

Meanwhile, the drag signal variation with the time shows that the sine load is another input form. To ascertain the frequency of input load, the modal analysis is conducted to acquire the natural frequency of the force balance. Furthermore, the finite element models are the same as virtual calibration. The results are characterized in Figure 7 and Table 1. For the single component force balance, the vibration in drag direction is the first mode and the corresponding natural frequency is 94.21Hz. For the three components balance, the vibration in drag, lift and pitching direction are the first, second and fifth mode and whose natural frequencies are 381.54Hz, 601.02Hz and 1467Hz, respectively. As known to all, the frequency is negative correlate with mass. In other words, the frequency of the force-measurement system will lower than the balance alone. Therefore, the frequency of input is half times of the natural frequency correspondingly.

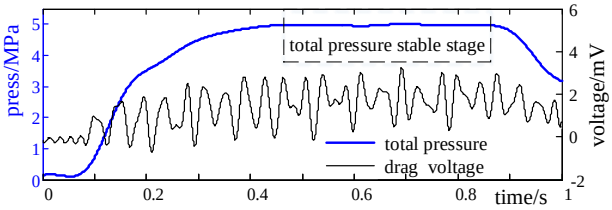

Figure 6 Total pressure and drag signal of impulse wind tunnel

Table 1 Natural frequency and mode shape of single and three components balance

mode no.	single component balance		three components balance	
	natural frequency	mode description	natural frequency	mode description
1	94.21Hz	Drag in direction F_x	381.54Hz	drag in direction F_x
2	635.08Hz	lift in direction F_y	601.02Hz	lift in direction F_y
3	796Hz	sideslip in direction F_z	903.2Hz	sideslip in direction F_z
4	1214.9Hz	rolling in direction M_x	1115.3Hz	rolling in direction M_x
5	1610.6Hz	yawing in direction M_y	1467Hz	pitching in direction M_z
6	1951.7Hz	pitching in direction M_z	1951.7Hz	yawing in direction M_y

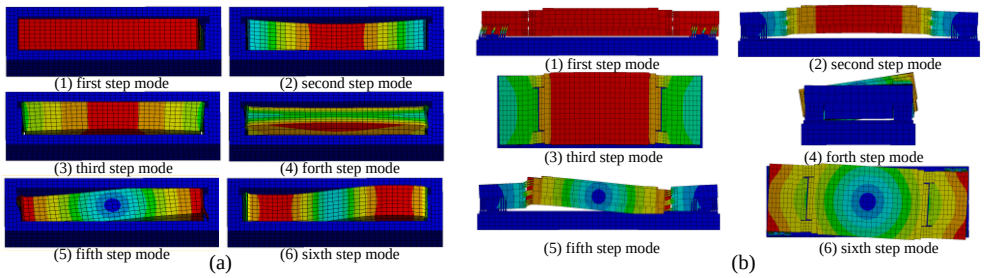

Figure 7 The mode shapes of force balance (a) single component balance (b) three components balance

4.3. The Rayleigh damping parameter calculation

There are many theories of the damping are advanced in the past few years [20,21], the Rayleigh theory is widely used in the finite element method, it is depicted as following:

$$\boldsymbol{C} = \alpha \boldsymbol{M} + \beta \boldsymbol{K} \tag{3}$$

Pan [22] calculate Rayleigh parameters α and β in the following equation.

$$\begin{bmatrix} \alpha \\ \beta \end{bmatrix} = \frac{2\omega_i \omega_j}{\omega_j^2 - \omega_i^2} \begin{bmatrix} \omega_j & -\omega_i \\ -\frac{1}{\omega_j} & \frac{1}{\omega_i} \end{bmatrix} \begin{bmatrix} \xi_i \\ \xi_j \end{bmatrix} \tag{4}$$

Where, ω_1 and ω_2 are the start and stop frequencies of the interesting vibration, ξ_1 and ξ_2 are the viscous damping coefficients which range from 0.03 to 0.05 for general mechanical systems. It is assumed that ξ_1 and ξ_2 are equal to 0.04 in this paper. Then, Rayleigh parameter is determined and listed

in Table 2.

Table 2 The damping parameters calculated through the Rayleigh method

Parameter	Single component balance		Three components balance	
	Step load	1/2*f* sine load	Step load	1/2*f* sine load
ω_1	0	0	350	200
ω_2	100	50	1500	1500
α	0	0	142.65	88.7
β	1.275×10^{-4}	2.546×10^{-4}	6.88×10^{-6}	7.49×10^{-6}

4.4 The inertia load calculate method

It is an impossible task to acquire accurate inertia load since the float frame would bear flexible deformation more or less. However, the lower order modes show that the float frame mainly vibrate as a whole. So it is feasible to substitute the accelerate of the float frame with some points. A1~A4 and A1~A6 in Figure 3 are the accelerate detect points of the balance. And the inertia load computing method is as following:

$$\boldsymbol{F}_I=\boldsymbol{M}\cdot\boldsymbol{A} \tag{5}$$

For the single component balance, m=7.728 kg, $A=1/4\times(A1_x+A2_x+A3_x+A4_x)$. And for the three components balance,

$$\boldsymbol{M}=\begin{pmatrix} m_x & & \\ & m_y & \\ & & J_z \end{pmatrix}=\begin{pmatrix} 26.71 & & \\ & 17.82 & \\ & & 0.134 \end{pmatrix},$$

$$\boldsymbol{A}=\begin{pmatrix} a_x \\ a_y \\ a_{Mz} \end{pmatrix}=\begin{pmatrix} 1/6 & 1/6 & 1/6 & 1/6 & 1/6 & 1/6 \\ 1/6 & 1/6 & 1/6 & 1/6 & 1/6 & 1/6 \\ 1/4 & 1/4 & -1/4 & -1/4 & 0 & 0 \end{pmatrix}\begin{pmatrix} A1_x & A2_x & A3_x & A4_x & A5_x & A6_x \\ A1_y & A2_y & A3_y & A4_y & A5_y & A6_y \\ A1_z & A2_z & A3_z & A4_z & A5_z & A6_z \end{pmatrix}^T.$$

4.5 Transient analysis result of the single component balance

Figure 8 illustrates the analysis results of the single component balance under step and half-frequency sine loading. Figure 8(a1) shows the input load, there is no load exerted in the period of time 0~50 ms, and is exerted in the period of time 50~50.2 ms. The corresponding drag load increased from 0 to 1,000 N, and it is kept constant in the period of time 11~300 ms. Figure 8(a2) shows the elastic and inertia load outputs. And Figure 8(a3) shows the sum of the elastic and inertia load. This figure shows that the deviation reduced sharply after inertia compensation with the amplitudes is 1,035N.

Figure 8(b1) shows the input load, show the drag input load history. The frequencies of the drag load are 47 Hz and the amplitude are 1,000 N. The load exerting time is divided into three stages. The startup time falls into 0~50 ms, in which the loads are zero. The load exerting time falls into 50~250 ms. The end stage falls into 250~350 ms, in which the loads are changed to zero. Figure 8(b2) shows the elastic and inertia load histories. And Figure 8(b3) shows the sum of the elastic and inertia load. This figure shows that the deviation reduced sharply after the inertia compensation, too.

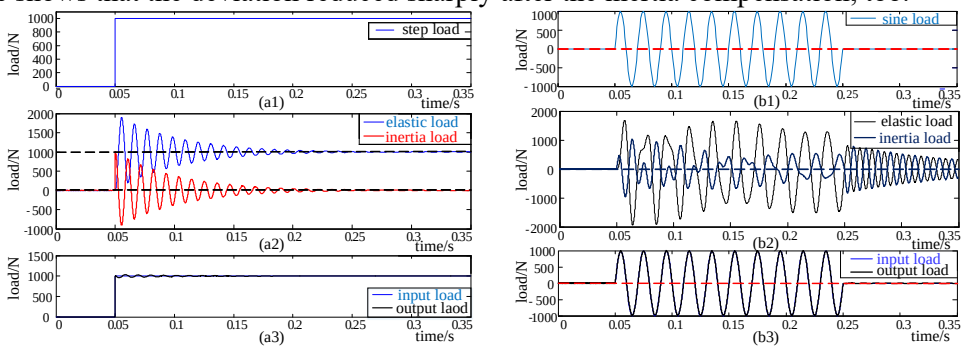

Figure 8 Analysis results of single component balance under step (a1)~(a3) and 1/2*f* sine (b1)~(b3) loading

4.6 Transient analysis result of the three components balance

Figure 9 illustrate the analysis result of the three components balance under step and half-frequency sine loading. Figure 9(a1) shows the input load, it is seen that the input loads are not exerted in the period of time 0~40 ms, and are exerted in the period of time 40~40.1 ms. The corresponding drag, lift load and pitching moment are increased from 0 to 1,000 N, 5,000 N and 1,000 Nm, respectively, and are kept in constant in the period of time 40.1~200 ms. Figure 9(a2) shows the elastic load output with the amplitudes of 1,989 N, 9,146 N and 1,797 Nm. Figure 9(a3) shows the inertia load output. And Figure 9(a4) shows the sum of above loads. This figure shows that the deviation reduced sharply after the inertia compensation with the amplitudes of three components are 1,163N, 5,574N and 1,038Nm.

Figure 9(b1) is input load, where 0~20 ms is start period, 20~70 ms is loading period during which the drag, lift load and the pitching moment are with the frequencies of 200Hz, 300Hz, 700Hz and the amplitudes of 1,000N, 5,000N, 1,000Nm, 70~100 ms the input load are changed to zero. Figure 9(b2) shows the elastic output with the amplitudes of 2,210N, 9,316N and 1,730Nm. Figure 9(b3) shows the inertia load output histories. And Figure 9(b4) shows the sum of elastic and inertia load. As shown in this figure, the frequency of the input and output is consistent with each other, also the transient amplitude is approximately the same in pitching moment, while has some deviation in the drag and lift. And the amplitudes of the drag, lift and the pitching moment are 1,024N, 5,376N and 1,071Nm, respectively.

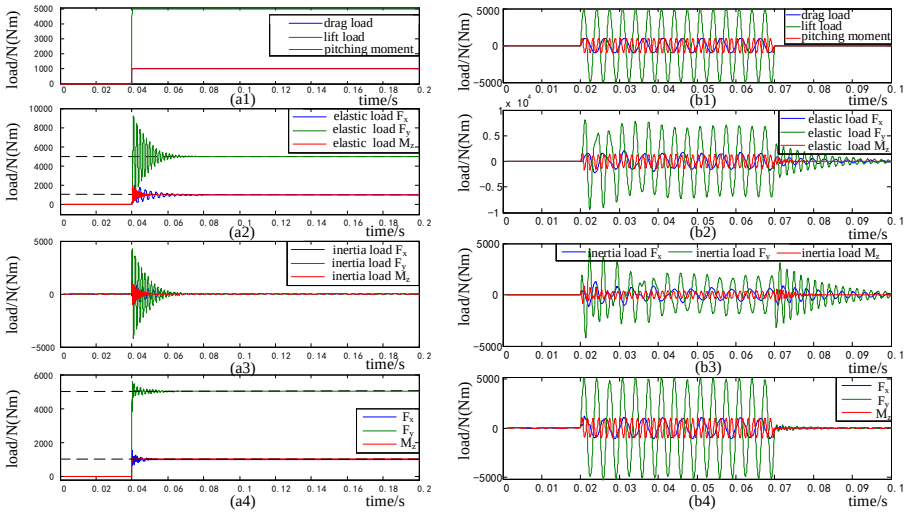

Figure 9 Analysis results of three components balance under step (a1)~(a4) and 1/2*f* sine (b1)~(b4) loading

5. Discussion of analysis result

5.1 Modal analysis result

Comparing the modal analysis results of the single and three components balance, it is obvious that the frequency of the single component balance is much lower than the three in drag direction. As known to all, the natural frequency of a structure embraces a negative correlation with mass and an active correlation with stiffness. Therefore, it is confident to declare the three components balance embrace a higher stiffness than the single one in drag direction.

5.2 Transient analysis result

Table 3 lists the mean value deviations of the single and three components force balance with and without the inertia compensation. For the single component balance, the deviations decrease one order of magnitude. For three components balance under step loading, the reduction of drag and lift is smaller than pitching moment. For the three components balance under sine loading, the reduction is one order of magnitude, too. This result prove that the inertia compensation method can improve the

accuracy of force measurement significantly while the mean value is regarded as the aerodynamic load.

Figure 10 describes the transient deviations between the input and output, where figure (a1) and (a2) show the deviations of the step and sine loading on single component balance, (b1) and (b2) are the deviations of the three components balance, respectively. For the single component balance, the transient deviations under step and sine loading are less than 50 N. For the three components balance under step loading, the drag, lift load and the pitching moment deviations are less than 170 N, 500 N and 50 Nm. So as to the sine loading, these deviations are less than 180 N, 480 N and 150 Nm. This means the transient deviation rates are less than 18, 9.6 and 15 percent. These results show that the transient output are improved significantly, too. Furthermore, the deviations of the single component balance are less than the three one. That is because the float frame of single component balance vibrate more similar to a rigid body since the stiffness of it is lower than the three one in drag direction. And this demonstrates that lower the stiffness will be good for the measurement and the inertia compensation.

Table 3 Mean value deviation before and after inertia component

inertia component	single component balance		three components balance					
	step loading	sine loading	step loading			sine loading		
	F_x(N)	F_x(N)	F_x(N)	F_y(N)	M_z(Nm)	F_x(N)	F_y(N)	M_z(Nm)
No	1.29	7.15	14.51	12.61	2.21	-8.69	-20.6	-1.54
Yes	0.2	0.12	5.88	8.19	0.17	0.679	-1.03	0.34

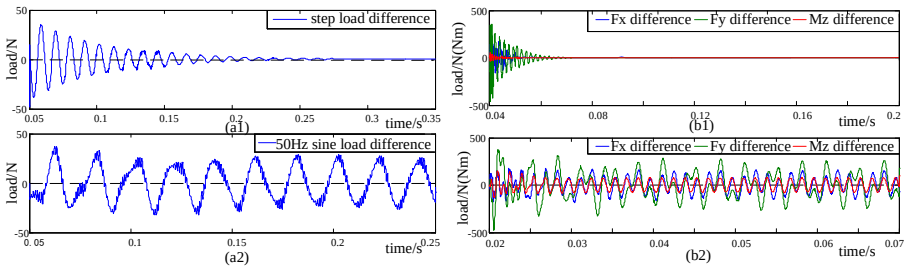

Figure 10 Transient deviations between input and output, step (a1) and sine (a2) loading of single component balance, step (b1) and sine (b2) loading of three components balance

6. Conclusion

This paper does research on the force balance including theoretical modeling, static virtual calibration, model analysis, transient analysis and the inertia compensation. Following conclusions could be drawn.

1. The dynamic equation and the simulation result prove that it is feasible to regard the mean value of elastic output as the aerodynamic load of the test model to some degree. To further improve the accuracy of force measurement, the inertia compensation is necessary.

2. The virtual static analysis results demonstrate that, the coupling between the drag and the pitching moment is more strong and between the lift and the drag or pitching moment is relatively weak.

3. The inertia compensation could reduce the transient deviation sharply for both the single and the three components balance, also these results after compensation could meet the need of transient force measurement

4. While meeting the requirement of safety and data analysis, lower the stiffness of a balance can improve the transient force measurement accuracy.

Acknowledgments

This research was finical supported by the Defense Key Laboratory of Science and Technology on Scramjet foundation Mianyang, Sichuan, China [grant numbers: STS/MY-ZY-2015-007].

References

[1] Stalker R J, A study of the free-piston shock tunnel, Dec 1967, AIAA Journal 5 2160-65.
[2] Sander T, Altenhofer P, Mundt C, Development of an MHD-augmented, high enthalpy, shock tunnel facility Mar, 1974, AIAA Journal 12 289-97.
[3] Olivier H, Gronig H, Hypersonic model testing in a shock tunnel, Feb 1995, AIAA Journal 33 262-65.
[4] Robinson M J, Mee D J, Tsai C Y, et al, Three-component force measurements on a large scramjet in a shock tunnel, Mar 2004, Journal of Spacecraft and Rockets 41 416-25.
[5] Schultz I A, Goldenstein C S, Strand C L, et al, Hypersonic scramjet testing via diode laser absorption in a reflected shock tunnel, June 2014, Journal of Propulsion and Power 30 1586-94.
[6] Tanno H, Kodera M, Komuro T, et al, Aerodynamic force measurement on a large-scale model in a short duration test facility, Feb 2005, Review of Scientific Instruments 76 035107.
[7] Tanno H, Komuro T, Sato K, et al, Aerodynamic force measurement technique with accelerometers in the impulsive facility HIEST, 2008, Shock Waves2008 471-76.
[8] Tanno H, Komuro T, Takahashi M, et al, Unsteady force measurement technique in shock tubes, Feb 2004, Review of Scientific Instruments 75 532-36.
[9] Singh P., Menezes V, Irimpan K J, Hosseini H, Impulse force balance for ultrashort duration hypersonic test facilities, 2015, Shock and Vibration. 2015 803253.
[10] Singh P, Trivedi S, Menezes V, Hosseini H. Dynamic calibration and validation of an accelerometer force balance for hypersonic lifting models, June 2013, The Scientific World Journal 2014 813759.
[11] Naumann K W, Ende H, Mathieu G, George A, Millisecond aerodynamic force measurement with side-jet model in the ISL shock tunnel, June 1993, AIAA Journal 31 1068-74.
[12] Saravanan S, Jagadeesh G, Reddy K P J, Aerodynamic force measurement using 3-component accelerometer force balance system in a hypersonic shock tunnel, 2009, Shock Waves. 18 425-35
[13] Smith A L, Mee D J, Daniel W J T, Shimoda T, Design, modelling and analysis of a six component force balance for hypervelocity wind tunnel testing, 2001, Computer and Structures 79 1077-88.
[14] Sahoo N, Suryavamshi K, et al, Dynamic force balances for short-duration hypersonic testing facilities, 2005, Experiments in Fluids 38 606-14.
[15] Laurence S J., Karl S, An improved visualization-based force-measurement technique for short-duration hypersonic facilities, 2010, Exp Fluids 48 949-65.
[16] Laurence S J, Hornung H G, Image-based force measurement in hypersonic facilities, 2009, Exp Fluids 46 343-53.
[17] Collopy A X, Lee S W, Development of dynamic force measurement capabilities at AEDC tunnel 9, in: 52rd AIAA Aerospace Sciences Meeting, National Harbor, Maryland, Jan, 2014, AIAA 2014-0983.
[18] Wang Y P, Liu Y F et al, Force measurement using strain-gauge balance in a shock tunnel with long test duration, May 2016, Review of Scientific Instruments 87, 055108.
[19] Wang Y, Liu Y, Jiang Z, Design of a pulse-type strain gauge balance for a long-test-duration hypersonic shock tunnel, 2016, Shock Wave. 26 835-44.
[20] Gounaris G D, Anifantis N K, Structural damping determination by finite element approach, 1999. Computers and structures 73 445-52.
[21] Spears R E, Jensen S R, Approach for Selection of Rayleigh Damping Parameters Used for Time History Analysis, 2012. Journal of Pressure Vessel Technology. 134 061801.
[22] Pan D G, Chen G D, Wang Z C. Suboptimal Rayleigh damping coefficients in seismic analysis of viscously-damped structures, 2014. Earthquake Engineering and Engineering Vibration. 13 653-70.